

The effect of C-vacancy on hydrogen storage and characterization of H₂ modes on Ti functionalized C₆₀ fullerene A first principles study

Ahmad S. Shalabi · Atef M. El Mahdy · Hayam O. Taha

Received: 23 August 2012 / Accepted: 28 September 2012 / Published online: 17 November 2012
© Springer-Verlag Berlin Heidelberg 2012

Abstract Density functional theory calculations were performed to examine the effect of a C vacancy on the physisorption of H₂ onto Ti-functionalized C₆₀ fullerene when H₂ is oriented along the *x*-, *y*-, and *z*-axes of the fullerene. The effect of the C vacancy on the physisorption modes of H₂ was investigated as a function of H₂ binding energy within the energy window (−0.2 to −0.6 eV) targeted by the Department of Energy (DOE), and as functions of a variety of other physicochemical properties. The results indicate that the preferential orientations of H₂ in the defect-free (i.e., no C vacancy) C₆₀TiH₂ complex are along the *x*- and *y*-axes of C₆₀ (with adsorption energies of −0.23 and −0.21 eV, respectively), making these orientations the most suitable ones for hydrogen storage, in contrast to the results obtained for defect-containing fullerenes. The defect-containing (i.e., containing a C vacancy) C₅₉TiH₂ complex do not exhibit adsorption energies within the targeted energy range. Charge transfer occurs from Ti 3*d* to C 2*p* of the fullerene. The binding of H₂ is dominated by the pairwise support–metal interaction energy $E(i)^{C_n \dots Ti}$, and the role of the fullerene is not restricted to supporting the metal. The C vacancy enhances the adsorption energy of Ti, in contrast to that of H₂. A significant reduction in the energy gap of the pristine C₆₀ fullerene is observed when TiH₂ is adsorbed by

it. While the C_{*n*} fullerene readily participates in nucleophilic processes, the adjacent TiH₂ fragment is available for electrophilic processes.

Keywords C vacancy · Hydrogen storage · Characterization · Ti-functionalized fullerene

Introduction

Hydrogen is a new renewable and clean energy option that is convenient, safe, and versatile. However, safe, efficient, and effective storage systems for molecular hydrogen are required that meet the Department of Energy (DOE) targets of 9.0 wt% and 81 g L^{−1} by 2015 for molecular applications. From a thermodynamic point of view, the hydrogen binding energy should be about −0.2 to −0.6 eV per hydrogen molecule, so that hydrogen can be adsorbed and desorbed under near-ambient conditions, and hydrogen release should be reversible [1].

The storage of gases in solids is a technological approach that is attracting great attention because of its many important applications [2, 3]. The physisorption of dihydrogen within a light, porous, and robust material is especially attractive, since it maximizes the possibility of highly reversible gas storage with fast kinetics and stability over multiple cycles. The use of fullerene materials for hydrogen storage has therefore gained attention. Fullerenes are a class of carbon molecules in which the carbon atoms are arranged into 12 pentagonal faces and two or more hexagonal faces. These fullerene molecules can take the form of spheres. Spherical fullerenes are often referred to as “buckyballs.” The terms fullerene and buckyball derive from the name of

A. S. Shalabi (✉)
Department of Chemistry, Faculty of Science, Benha University,
P.O.Box 13518, Benha, Egypt
e-mail: asshalabi@hotmail.com

A. M. El Mahdy · H. O. Taha
Department of Physics, Faculty of Education,
Ain Shams University,
Cairo, Egypt

the architect Richard Buckminster Fuller. Each spherical fullerene is hollow, and the smallest spherical fullerene is constructed from 32 carbon atoms. An overview of fullerenes is given in [4, 5].

There are several advantages of using fullerenes for hydrogen-storage applications [6]. C_{60} buckyballs show no capacity to store hydrogen. However, theoretical calculations have shown that decorating C_{60} and other buckyballs with transition metal atoms leads to species that show extensive hydrogen storage. In these species, the hydrogen is bonded through the Kubas interaction, and the nature of this bonding is explained by the Dewar–Chatt–Duncanson model [7]. Fullerenes can be prepared with high purity, and their curvature helps to avoid clustering, thus encouraging the metal dopants to remain isolated. Several studies have shown that the binding strength of molecular hydrogen with nanoscale carbon structures can be substantially enhanced by adsorbing transition metals such as Ti onto the surface of the structure. Zhao et al. [8] carried out calculations on C_{60} and $C_{48}B_{12}$ samples and found that charge transfer interactions should allow the formation of stable organometallic buckyballs with transition metals. Yildirim et al. [9] investigated molecular and dissociative adsorption of multiple hydrogen molecules on transition metal decorated C_{60} . They showed that Ti prefers the hollow sites in the hexagons of C_{60} (binding energy: -2.1 eV), and once the metal is adsorbed onto C_{60} it can bind up to four hydrogen molecules with a binding energy of -0.465 eV/ H_2 . Sun et al. [10] considered the clustering of Ti on a C_{60} surface and its effect on hydrogen storage. They showed that the preferred position for Ti was a hexagonal site (with a binding energy of 2.35 eV), and once adsorbed, the Ti was able to bind hydrogen molecules with a binding energy of -0.55 eV/ H_2 . They also showed that clustering reduced this interaction energy to -0.38 eV/ H_2 . However, neither theoretical nor experimental data regarding the adsorption of H_2 on Ti deposited onto pure C_{60} fullerene or C_{60} with a C vacancy are available to compare with our data. Our results may therefore serve as theoretical predictions.

The main objectives of the study described in the present paper were to examine the effect of a C vacancy in Ti-functionalized C_{60} fullerene on its capacity to store hydrogen and to characterize the preferential adsorption modes of H_2 onto this fullerene. We considered two types of complexes: defect-free $C_{60}TiH_2$ (without a C vacancy) and defect-containing $C_{59}TiH_2$ (with a C vacancy). An adsorption site on top of a C atom in the fullerene was selected for the TiH_2 fragment in order to examine the effect of the C vacancy. Theoretical characterization involved studying the physical adsorption of H_2 within the energy window targeted by the Department of Energy (DOE), the charge transfer from Ti to the fullerene, pairwise and non-pairwise additivity, frontier orbital energy gaps and isosurface plots, the density of states, molecular electrostatic potentials, and simulated infrared (IR), Raman (R), and proton nuclear magnetic resonance (1H NMR) chemical shifts.

Computational details

The C_{60} fullerene molecule considered here consisted of 60 carbon atoms bonded in a near-spherical configuration. This shape, called a truncated icosahedron, contains 20 hexagons, 12 pentagons, 30 carbon double bonds, and 60 carbon single bonds, and its diameter is about 7 \AA (Fig. 1). The subsequent reactions of molecular hydrogen with the Ti atom deposited on top of a C atom and the corresponding C vacancy were examined, and three different orientations for H_2 (in the x -, y -, and z -directions) were considered (Fig. 2). To determine the equilibrium geometries of the C_nTiH_2 complexes, we carried out the following steps: (1) full geometry optimization of the pristine C_{60} was performed at the B3LYP/6-31G(d) level of theory; (2) the vertical distance between Ti and the top of the C atom was optimized; (3) the vertical distance between the center of mass of H_2 and Ti was optimized; and finally (4) the internuclear distance in H_2 was optimized. Steps (2)–(4) were carried out at the Hartree–Fock (HF) level with the small LANL2MB basis set. The optimal geometries obtained were then refined by performing

Fig. 1 Side views of the two considered types of pristine C_n fullerenes (without adsorbed TiH_2 groups): **a** defect free C_{60} fullerene (without a C vacancy); **b** defect containing C_{59} fullerene (with a C vacancy)

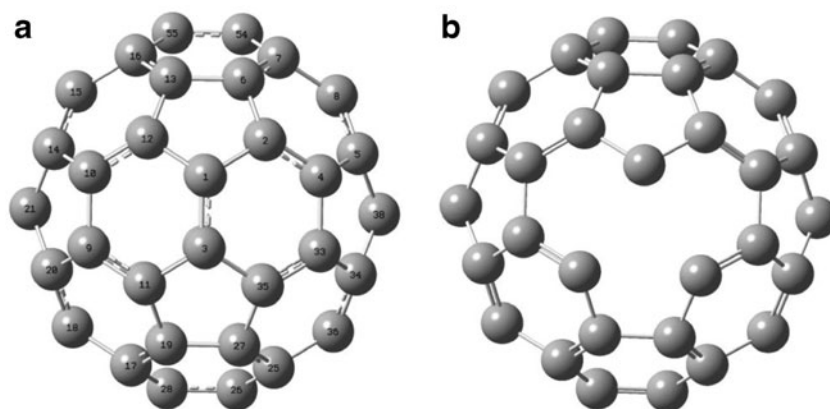
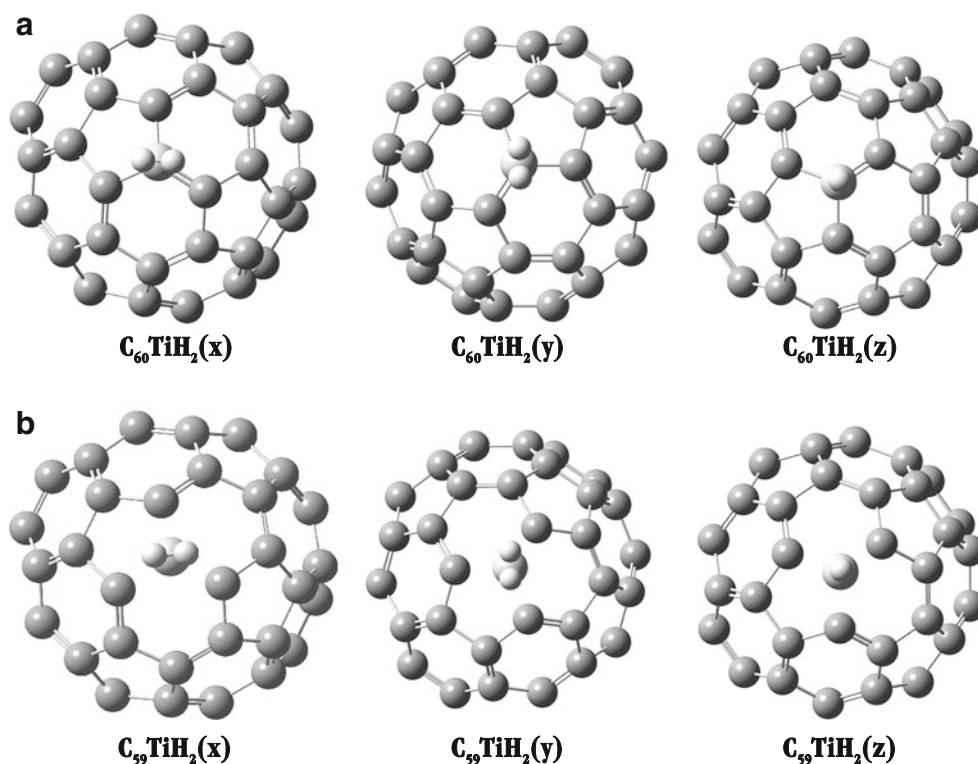


Fig. 2 Optimized geometries of $C_{60}TiH_2$ and $C_{59}TiH_2$ complexes with H_2 oriented parallel to the x -, y -, and z -axes of the fullerene



single point energy calculations at the B3LYP/6-31G(d) level of theory to determine adsorption energies and predict properties. Steps (2)–(4) were repeated for the defect-containing $C_{59}TiH_2$ complexes. The LANL2MB basis set places STO-3G on the first-row atoms, and the Los Alamos ECP plus MBS on Na–La and Hf–Bi [11]. The 6-31G(d) basis set is that of Petersson and coworkers, defined as part of the Complete Basis Set methods, with a single diffuse function [12]. The B3LYP hybrid functional was chosen since it provides a rather accurate description of metal interactions, and for magnetic systems it provides a reasonable (albeit imperfect) picture that lies midway between the HF and pure gradient-corrected approximation (GGA) descriptions [13, 14]. In some cases the differences between the experimental values and the calculated ones can be considered to be due to systematic error [15]. B3LYP correctly reproduces the thermochemistry of many compounds, including transition metal atoms [16–18], and ensures that the electronic ground states of first-row transition metals and the energy difference between low-lying electronic states with different spin multiplicities are accurately described [19, 20].

The energy of the adsorption of H_2 onto the Ti-functionalized C_{60} (without a C vacancy) or C_{59} (with a C vacancy) fullerene was obtained from the relations

$$\Delta E_{\text{ads.}}(H_2) = E(C_{60}TiH_2) - E(C_{60}Ti) - E(H_2) \quad (1)$$

$$\Delta E_{\text{ads.}}(H_2) = E(C_{59}TiH_2) - E(C_{59}Ti) - E(H_2), \quad (2)$$

where $\Delta E_{\text{ads.}}(H_2)$ is the adsorption energy of H_2 , $E(C_nTiH_2)$ is the total electronic energy of the complex, $E(C_nTi)$ is the electronic energy of the Ti-functionalized C_n , and $E(Ti)$ is the electronic energy of the free Ti atom. According to the preceding definitions, a negative value of $\Delta E_{\text{ads.}}(H_2)$ corresponds to exothermic adsorption. The calculations were carried out using the Gaussian 09 software package [21], and the figures were generated using the associated GaussView software.

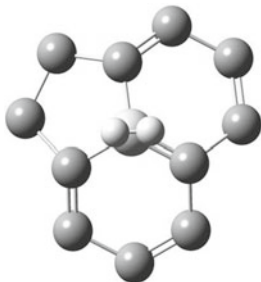
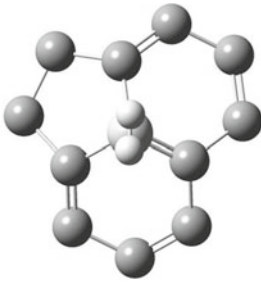
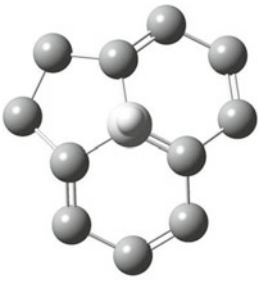
Results and discussion

Physisorption of molecular hydrogen

Tables 1 and 2 show the results of optimizing the adsorption of Ti and H_2 onto C_{60} , including the adsorption energies ($\Delta E_{\text{ads.}}$) and vertical distances (d). Mulliken charges on Ti atoms (Q_{Ti}) are also included. We first analyze the energy for the adsorption of H_2 onto $C_{60}TiH_2$ complexes (i.e., no C vacancy); see Table 1. The adsorption energies for molecular hydrogen oriented along the x -, y -, and z -axes of C_{60} are exothermic. While the adsorption energy of H_2 oriented along the x - and y -axes (-0.23 and -0.21 eV) are characterized as being in the energy range required for H_2 storage at room temperature (-0.2 to -0.6 eV), as suggested by Strobel et al. [22], the adsorption energy of H_2 oriented along the z -axis (-0.03 eV) is outside of this range. The adsorption energies of H_2 oriented along the x - and y -axes also present the smallest distances between C_{60} and Ti and between Ti and the center of mass of

Table 1 Interatomic distances ($d(\text{C}_{60}\text{-Ti})$, $d(\text{Ti-H}_2)$, $d(\text{H-H})$), adsorption energies ($\Delta E_{\text{ads.}}(\text{H}_2)$), and Mulliken charges (Q_{Ti}) of $\text{C}_{60}\text{TiH}_2$ complexes

	$\text{C}_{60}\text{TiH}_2(\text{x})$	$\text{C}_{60}\text{TiH}_2(\text{y})$	$\text{C}_{60}\text{TiH}_2(\text{z})$
$d(\text{C}_{60}\text{-Ti})$	2.23 Å	2.25 Å	2.51 Å
$d(\text{Ti-H}_2)$	2.01 Å	1.99 Å	6.39 Å
$d(\text{H-H})$	0.75 Å	0.76 Å	0.70 Å
$\Delta E_{\text{ads.}}(\text{H}_2)$	-0.23 eV	-0.21 eV	-0.03 eV
Q_{Ti}	0.28 e	0.32 e	0.21 e

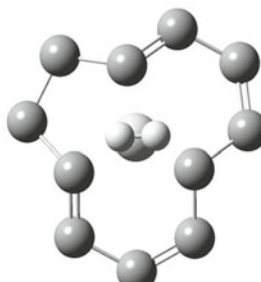
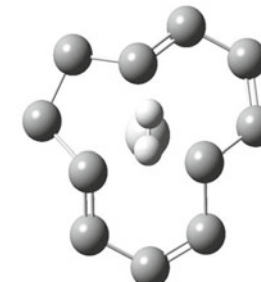
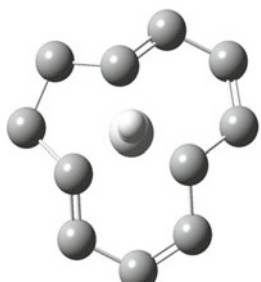




H_2 , and the largest amount of charge transfer from Ti $3d$ to C $2p$, leading in turn to the most extensive hybridization of atomic orbitals. While the experimental H–H distance (0.74 Å) is elongated under the effect of H_2 adsorption along the x - and y -axes, it is shortened by H_2 adsorption along the z -axis. According to Yildirim and Ciraci [23], Ti contributes only d electrons; electrons are almost absent from Ti $4s$ —they are probably promoted to Ti d orbitals. When a metal atom is supported on the fullerene, the large electronegativity of C_{60} facilitates the transfer of electrons from the metal atom to C_{60} , leaving the metal atom in the cationic form. Hence, molecular

hydrogen can be trapped by the metal ion through a charge polarization mechanism. Both filled and empty d orbitals are necessary for metal–hydrogen complex formation. Consequently, heavy transition metals with diffuse d orbitals, such as Pt and Pd, are not good candidates for molecular adsorption. Yildirim and Ciraci also proposed that such metals can interact strongly with the σ^* antibonding orbital of the H_2 molecule, destabilizing the structure of dihydrogen, thus promoting classical hydride formation. We can therefore conclude that a light transition metal such as Ti is a good candidate for the molecular adsorption of H_2 . Also note that

Table 2 Interatomic distances ($d(\text{C}_{59}\text{-Ti})$, $d(\text{Ti-H}_2)$, $d(\text{H-H})$), adsorption energies ($\Delta E_{\text{ads.}}(\text{H}_2)$), and Mulliken charges (Q_{Ti}) of $\text{C}_{59}\text{TiH}_2$ complexes

	$\text{C}_{59}\text{TiH}_2(\text{x})$	$\text{C}_{59}\text{TiH}_2(\text{y})$	$\text{C}_{59}\text{TiH}_2(\text{z})$
$d(\text{C}_{59}\text{-Ti})$	1.01 Å	1.01 Å	1.01 Å
$d(\text{Ti-H}_2)$	2.60 Å	2.60 Å	2.84 Å
$d(\text{H-H})$	0.73 Å	0.72 Å	0.72 Å
$\Delta E_{\text{ads.}}(\text{H}_2)$	-0.14 eV	-0.14 eV	-0.05 eV
Q_{Ti}	0.97 e	0.97 e	0.99 e

the experimental H–H distance (0.74 Å) is neither significantly shortened nor elongated under the effect of H₂ adsorption. According to [23], when a single H₂ molecule is introduced onto t80Ti, Ti is able to donate just enough charge to the σ* antibonding state to cause dihydrogen to be unstable with respect to the dissociation of H₂. However, when more hydrogen molecules are added to the system, the charge transfer per H₂ molecule is not enough to destabilize the dihydrogen state, and therefore the absorption becomes molecular. The amount of charge transferred from the Ti atom and the H–H bond length (see Table 1) suggest that we are dealing with the nondissociative adsorption of H₂.

When we consider the energy of the adsorption of H₂ on Ti-functionalized C₅₉ with a C vacancy (Table 2), it is clear that the adsorption energies of molecular hydrogen oriented along the x-, y-, and z-axes of C₅₉ are also exothermic (−0.14, −0.14, and −0.05 eV). However, they are not in the target energy range allowing hydrogen storage at room temperature (−0.2 to −0.6 eV). While the calculated parameters of H₂ oriented along the x- and y-axes are identical, they only differ from those of H₂ oriented along the z-axis in the distance between Ti and the center of mass of H₂, and in the value of the adsorption energy. The z-orientation is characterized by an elongated distance and a smaller adsorption energy. The experimental H–H distance (0.74 Å) was not significantly shortened by the adsorption of H₂ along the x-, y-, and z- axes.

We now consider the effect of a C vacancy on the structures and energetic properties of the C₆₀TiH₂ and C₅₉TiH₂ complexes. The distance between Ti and C₅₉ is significantly shorter than the distance between Ti and C₆₀ due to the absence of electronic repulsive effects between Ti 3*d* and C 2*p*. The amount of charge transfer from Ti to C₅₉ is significantly larger than that from Ti to C₆₀ due to the absence of the C 2*p* atomic orbital at vacancy. While the adsorption energies of two of the three orientations of H₂ on Ti-functionalized C₆₀ were within the DOE-targeted energy window for hydrogen storage, none of the adsorption energies of the H₂ orientations on Ti-functionalized C₅₉ were within this desirable energy range. The values of the structural and energetic properties examined here vary among the H₂-adsorption modes of Ti-functionalized C₆₀, meaning that these properties characterize each H₂-adsorption mode of Ti-functionalized C₆₀. This is not the case for Tifunctionalized C₅₉.

Pairwise and non-pairwise additivity

While the concept of non-additivity has been studied for atom clusters, insulators, and SWCNTs [24–27], it has been completely overlooked for fullerenes. We define the interaction energy $E(i)^{C60...Ti...H2}$ among three subsystems—the fullerene support (C₆₀), the metal (Ti), and the (H₂) molecule—as

$$E(i)^{C60...Ti...H2} = E^{C60...Ti...H2} - E^{C60} - E^{Ti} - E^{H2}, \tag{3}$$

where every energy term on the right-hand side of Eq. 3 is calculated using the geometrical parameters that belong to the equilibrium geometry of C₆₀...Ti...H₂. $E(i)^{C60...Ti...H2}$ is the energy required to separate the three subsystems without changing their geometrical parameters. This energy can be decomposed into three pairwise additive components and a non-additive term E^{nadd} :

$$E(i)^{C60...Ti...H2} = E(i)^{C60...Ti} + E(i)^{C60...H2} + E(i)^{Ti...H2} + E^{nadd} \tag{4}$$

where

$$E(i)^{A...B} = E^{A...B} - E^A - E^B (A \neq B = S, Ti, H_2), \tag{5}$$

and no geometrical relaxation is allowed within a subsystem. The non-additivity term E^{nadd} [28] is a measure of the cooperative interactions among the subsystems,

where

$$E(i)^{C60...Ti} = E^{C60...Ti} - E^{C60} - E^{Ti} \tag{6}$$

$$E(i)^{Ti...H2} = E^{Ti...H2} - E^{Ti} - E^{H2} \tag{7}$$

$$E^{nadd} = E(i)^{C60...Ti...H2} - E(i)^{C60...Ti} - E(i)^{C60...H2} - E(i)^{Ti...H2} \tag{8}$$

In Tables 3 and 4, the total interaction energies of the C₆₀...Ti...H₂ systems, the pairwise energy components, and the non-additive terms are given (as defined in Eqs. 3–8). The same set of equations (3–8) were also applied to the defect-containing complexes C₅₉...Ti...H₂.

In Table 3, the total interaction energies of C₆₀...Ti...H₂ complexes (without C vacancies) are seen to be dominated by the pairwise additive component $E(i)^{C60...Ti}$. An important issue in any study of a support–metal system is the extent to which the support (C₆₀) influences the interaction of an adsorbate (H₂) with the metal (Ti). The $E(i)^{C60...Ti}$ term is always greater than the $E(i)^{Ti...H2}$ term. This implies that the binding of H₂ is mostly dominated by the support–metal contribution $E(i)^{C60...Ti}$, followed by the pairwise metal–dihydrogen additive contribution $E(i)^{Ti...H2}$. We can therefore conclude that the C₆₀ support has a considerable effect on the interaction of H₂ with Ti, and its role is not restricted to supporting the metal. In other words, the adsorption

Table 3 Interaction energy components of C₆₀TiH₂ complexes. Total interaction energies: $E(i)^{C_{60}\dots Ti\dots H_2}$; pairwise components: $E(i)^{C_{60}\dots Ti}$, $E(i)^{C_{60}\dots H_2}$, $E(i)^{Ti\dots H_2}$; non-additivity term: ϵ^{nadd} ; all energies are in eV

	$E(i)^{C_{60}\dots Ti\dots H_2}$	$E(i)^{C_{60}\dots Ti}$	$E(i)^{C_{60}\dots H_2}$	$E(i)^{Ti\dots H_2}$	ϵ^{nadd}
C ₆₀ TiH ₂ (x)	-1.194	-0.968	-0.005	-0.187	-0.034
C ₆₀ TiH ₂ (y)	-1.158	-0.954	-0.003	-0.216	0.015
C ₆₀ TiH ₂ (z)	-0.590	-0.558	-0.004	-0.001	-0.027

energy of H₂ depends on the type of fullerene support (C_n) involved and the amount of charge transferred from the metal, which in turn depends on the electronegativity of the fullerene support. Moreover, the complexes C₆₀...Ti...H₂(x) and C₆₀...Ti...H₂(y), for which the H₂-adsorption energies (-0.23 and -0.21 eV) are in the energy range that permits hydrogen storage at room temperature (-0.2 to -0.6 eV), are characterized by larger $E(i)^{C_{60}\dots Ti}$ and $E(i)^{Ti\dots H_2}$ terms than those of the complex C₆₀...Ti...H₂(z), for which the H₂-adsorption energy (-0.03 eV) is not within the energy range that allows hydrogen storage at room temperature. However, the non-additivity term ϵ^{nadd} , which is a measure of the cooperative interactions among the subsystems, is not discriminative.

In Table 4, the total interaction energies of C₅₉...Ti...H₂ complexes (with C vacancies) are again seen to be dominated by the pairwise additive term $E(i)^{C_{59}\dots Ti}$, and the $E(i)^{C_{59}\dots Ti}$ term is always greater than the $E(i)^{Ti\dots H_2}$ term, implying that the binding of H₂ is dominated by the support-metal contribution $E(i)^{C_{59}\dots Ti}$, followed by the pairwise metal-dihydrogen additive contribution $E(i)^{Ti\dots H_2}$. The C₅₉ support therefore has a considerable effect on the interaction of H₂ with Ti, and its role is not restricted to supporting the metal. The complexes C₅₉...Ti...H₂(x) and C₅₉...Ti...H₂(y) have larger $E(i)^{Ti\dots H_2}$ and ϵ^{nadd} terms than those of the C₅₉...Ti...H₂(z) complex. The values for the other two terms, $E(i)^{C_{59}\dots Ti}$ and $E(i)^{C_{59}\dots H_2}$, are nearly identical for all three H₂ orientations, and are therefore not discriminative. Moreover, a comparison of Table 3 and Table 4 reveals that the C vacancy has an enormous effect on the total interaction energies of the complexes. The $E(i)^{C_n\dots Ti}$ values in Tables 1 and 2, together with the $\Delta E_{ads}(H_2)$

values in Tables 3 and 4, indicate that the C vacancy enhances the adsorption energy of Ti and decreases the adsorption energy of H₂.

Frontier orbitals

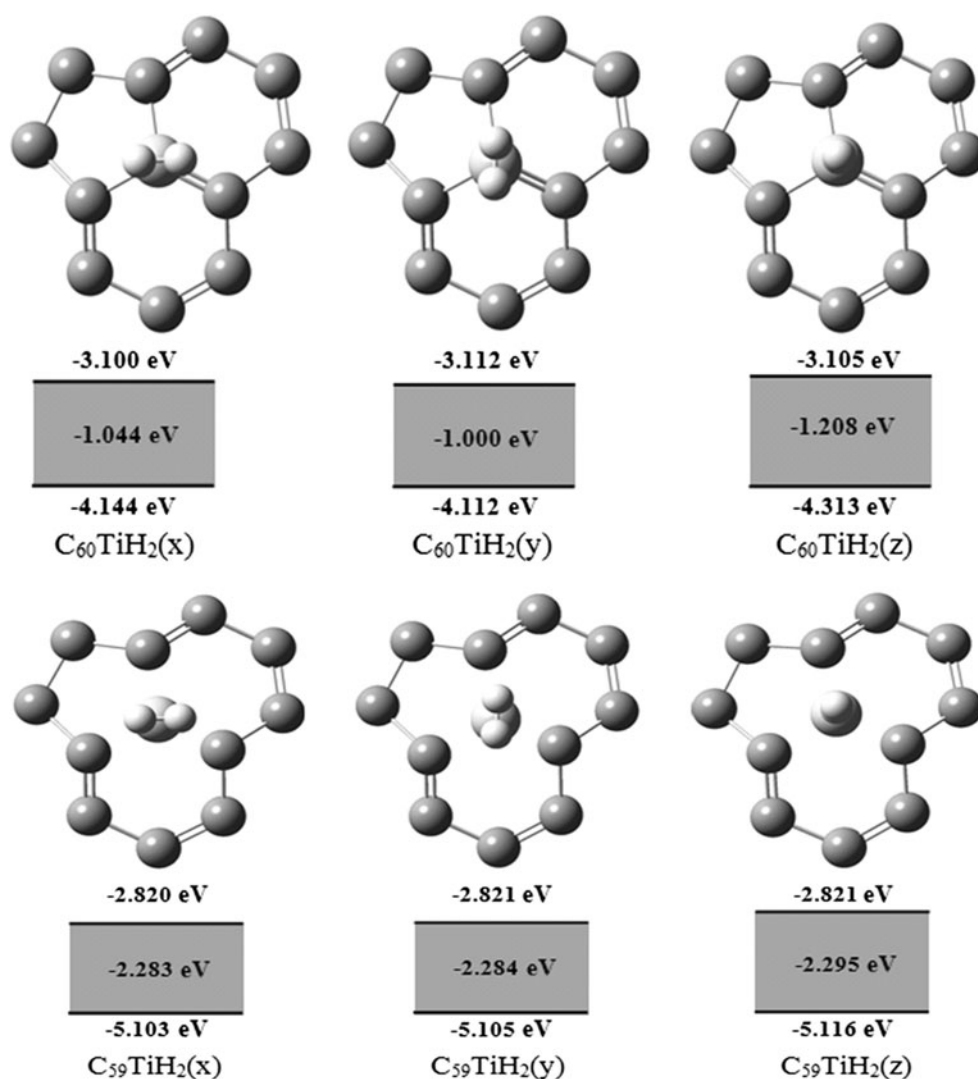
The energy difference between the highest occupied molecular orbital (HOMO) and the lowest unoccupied molecular orbital (LUMO) can be considered a good indicator of changes in electronic properties and chemical reactivity [29]. In general, band gaps are governed by molecular structure and the theoretical size of the band gap defines the transition (excitation) energy from the ground state to the first dipole-allowed excited state [30]. However, the crudest estimate—albeit the one most widely used due to its low computational cost—is based on the energy difference between the highest occupied molecular orbital (HOMO) and the lowest unoccupied molecular orbital (LUMO).

In solid state and condensed matter physics, the density of states (DOS) of a system describes the number of states per interval of energy at each energy level that can be occupied by electrons. A high DOS at specific energy level means that there are many states available for occupation at that level. The HOMO, LUMO, and HOMO-LUMO energy gaps of C₆₀TiH₂ and C₅₉TiH₂ complexes are presented in Fig. 3, and the corresponding density of states (DOS) are presented in Fig. 4. The HOMO-LUMO energy gaps of the pristine fullerenes were calculated to be -2.945 eV for C₆₀ (without a C vacancy), and -0.632 eV for C₅₉ (with a C vacancy). As can be seen from Fig. 3, a significant reduction in the energy gap is observed when the TiH₂ fragment is adsorbed onto the pristine C₆₀ fullerene. This reduction

Table 4 Interaction energy components of C₅₉TiH₂ complexes. Total interaction energies: $E(i)^{C_{59}\dots Ti\dots H_2}$; pairwise components: $E(i)^{C_{59}\dots Ti}$, $E(i)^{C_{59}\dots H_2}$, $E(i)^{Ti\dots H_2}$, and the non-additivity term: ϵ^{nadd} . All energies are given in eV

	$E(i)^{C_{59}\dots Ti\dots H_2}$	$E(i)^{C_{59}\dots Ti}$	$E(i)^{C_{59}\dots H_2}$	$E(i)^{Ti\dots H_2}$	ϵ^{nadd}
C ₅₉ TiH ₂ (x)	-10.966	-10.829	0.0057	0.128	-0.271
C ₅₉ TiH ₂ (y)	-10.966	-10.829	0.0058	0.131	-0.274
C ₅₉ TiH ₂ (z)	-10.875	-10.829	-0.0056	0.050	-0.091

Fig. 3 (*Upper views*): Overhead projection of H₂ deposited on Ti and oriented along the *x*-, *y*-, and *z*- axes of the defect free C₆₀ fullerene (without a C vacancy) and defect containing C₅₉ fullerene (with a C vacancy). (*Lower views*): HOMO and LUMO energy levels, and HOMO–LUMO energy gaps of the defect free C₆₀TiH₂ complexes (without C vacancies) and defect containing C₅₉TiH₂ complexes (with C vacancies)

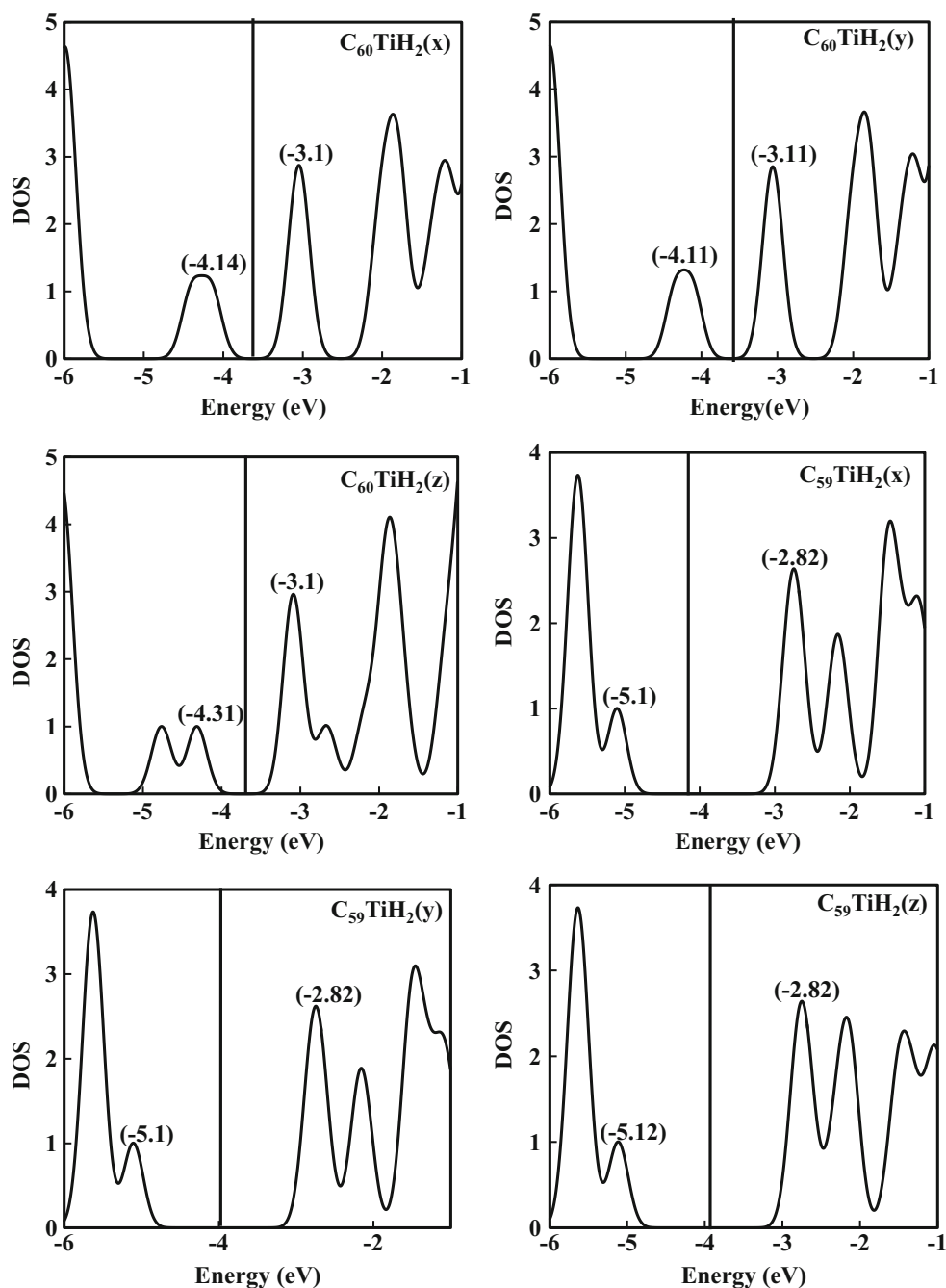


would be explained by a higher density of states near the Fermi level, which arises from the overlap of the 3*d* electrons of Ti and the π -electron system of the fullerene (Fig. 4). A smaller HOMO–LUMO gap should result in easier excitation of electrons from the low-lying occupied levels to the upper empty level, which in turn enhances chemical reactivity towards an adsorbate. A similar degree of partial charge transfer is expected, which can be ascribed to the electronic reorganization caused by the interaction of the C₆₀ and Ti. In other words, the presence of the 3*d* electrons of Ti in the antibonding orbitals of fullerene leads to an enhancement of the electron density in the fullerene and thus a smaller band gap [31]. Now consider the pristine C₅₉ fullerene (with a C vacancy); see Fig. 3. As can be seen, a significant increase in the energy gap is observed when the TiH₂ fragment is adsorbed. This increase can in turn be explained by a lower density of states near the Fermi level, which arises from the overlap of the 3*d* electrons of Ti and the π -electron system of the fullerene (Fig. 4). Moreover, in

Fig. 4 there are significant changes in the features of the density of states and the Fermi level when a C vacancy is introduced into the fullerene complex. While these changes distinguish the *x*- and *y*-orientations of H₂ from the *z*-orientation of the complex without a C vacancy, they cannot discriminate among the H₂ orientations of the complex with a C vacancy, as both the DOS features and Fermi levels are identical for all orientations in this case.

A larger HOMO–LUMO gap should mean that the excitation of electrons from the low-lying occupied levels to the upper empty level is less probable, which in turn will disfavor chemical reactivity towards an adsorbate. This explains the lower adsorption energies of H₂ in the complexes with C vacancies. As shown in Fig. 3, the complexes C₆₀TiH₂(*x*) and C₆₀TiH₂(*y*) without C vacancies have narrower band gaps than the complex C₆₀TiH₂(*z*). However, the band gaps of the complexes C₅₉TiH₂(*x*) and C₅₉TiH₂(*y*) with C vacancies are identical, do not differ significantly from that of the complex C₅₉TiH₂(*z*), and are not discriminative. Thus, the

Fig. 4 Density of states (DOS), HOMOs, LUMOs, and Fermi energy levels (vertical lines) of $C_{60}TiH_2$ and $C_{59}TiH_2$ complexes

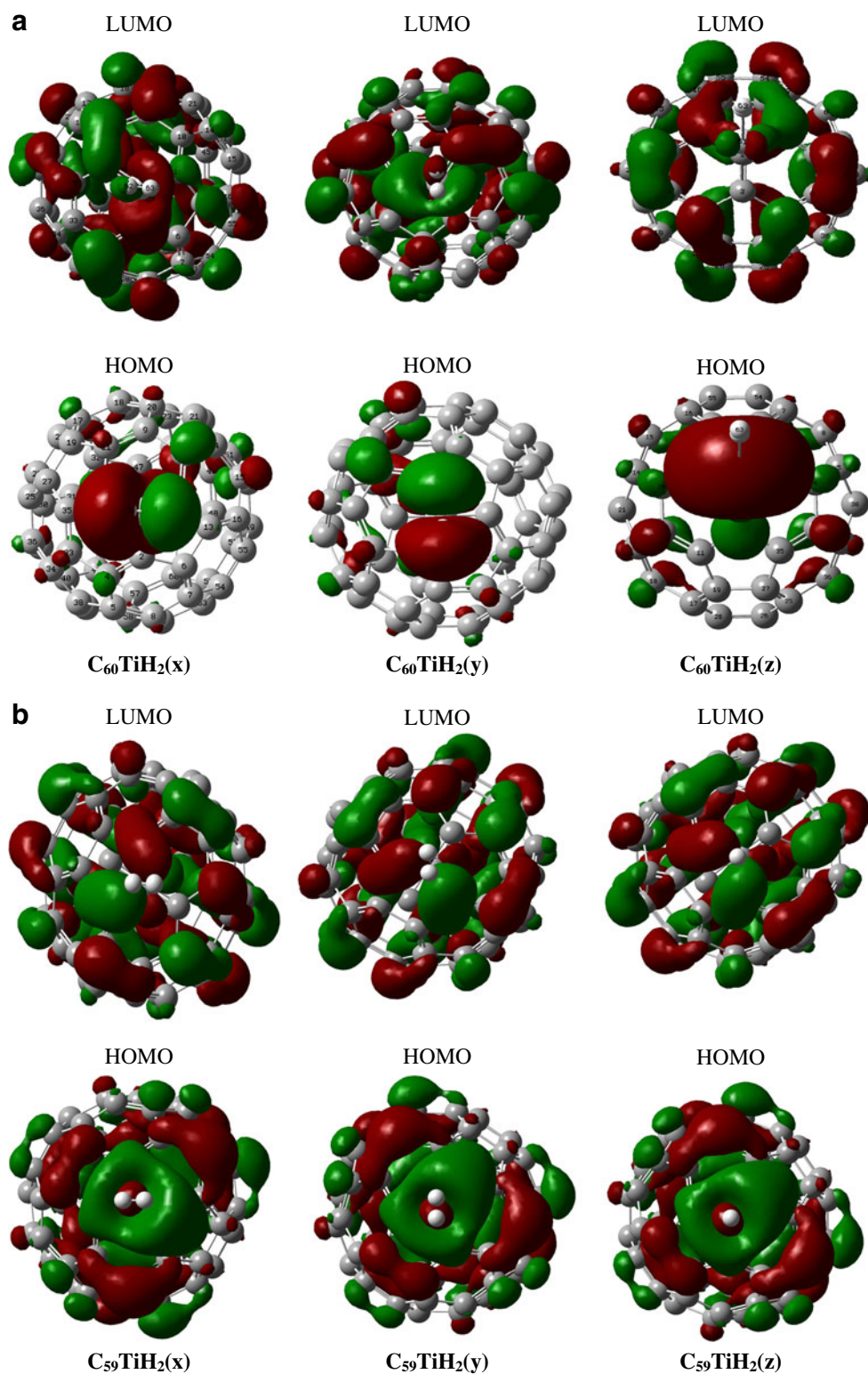


preferable orientations of H_2 are along the x - and y -axes of the fullerene in the defect-free complexes. Consequently, the occurrence of the H_2 -adsorption energy within the energy range permitting hydrogen storage at room temperature is dependent on the width of the band gap, the Fermi level, and the DOS.

An understanding of the distribution of frontier orbitals around fullerene complexes would be valuable as it could be used to guide the design and characterization of new functionalized fullerenes for hydrogen storage. Frontier orbital isosurface plots of the present complexes are presented in Fig. 5.

While there is strong localization of the HOMOs on the TiH_2 fragments of the $C_{60}TiH_2$ complexes, there is strong delocalization of the LUMOs on both the TiH_2 fragments and the inner and outer surfaces of the fullerene. This implies a significant flow of electronic charge across the interface between the TiH_2 fragment and the fullerene buckyball. While the overall features of the isosurface plots of $C_{60}TiH_2(x)$ and $C_{60}TiH_2(y)$ are very similar, they are very different from those of $C_{60}TiH_2(z)$. However, this is not the case for the $C_{59}TiH_2$ complexes: the isosurface plots could not be used to discriminate between the complexes $C_{59}TiH_2(x)$ and $C_{59}TiH_2(y)$ on

Fig. 5 Front views of frontier orbitals (HOMO and LUMO) isosurface plots of **a** defect free $C_{60}TiH_2$ complexes (without C vacancies); **b** defect containing $C_{59}TiH_2$ complexes (with C vacancies) in which H_2 is oriented along the x -, y -, or z -axis of the fullerene



the one hand and the complex $C_{59}TiH_2(z)$ on the other. Thus, the isosurface plots indicate that $C_{60}TiH_2(x)$ and $C_{60}TiH_2(y)$ complexes (without C vacancies) are the most suitable configurations for hydrogen storage, based on the recommended adsorption energy range.

MEPs

Molecular electrostatic potentials (MEPs) have been extensively used to guide the interpretation and prediction of molecular behavior [32]. They have been shown to be a

useful tool when studying both electrophilic and nucleophilic processes, in particular the “recognition” of one molecule by another [33, 34]. Electrostatic interactions play an important role in single-walled carbon nanotube (SWCNT) sensor investigations [35, 36]. Despite using different theoretical methodologies, several studies indicate that defect sites on SWCNTs are chemically more reactive than non-defect sites [37–39]. However, less theoretical attention has been paid to fullerenes in this context.

Molecular electrostatic potentials are either low negative potentials that are characterized by an abundance of electrons and reactivity with electrophiles, or high positive potentials that are characterized by an absence of electrons and reactivity with nucleophiles. We denote the former by a deep red color and the latter by a light yellow color. The molecular electrostatic potential surfaces of $C_{60}TiH_2$ and $C_{59}TiH_2$ complexes are given in Fig. 6. As shown, the intensities of the negative and positive MEPs of the complexes are affected by the orientation of H_2 . While the MEPs of the complexes $C_{60}TiH_2(x)$ and $C_{60}TiH_2(y)$ are similar, they are different from those of the complex $C_{60}TiH_2(z)$, where excess negative potentials surround the H_2 molecule. This indicates that the complexes $C_{60}TiH_2(x)$ and $C_{60}TiH_2(y)$ are less reactive with electrophiles. While the high positive potentials increase noticeably in the region of the buckyball, the low negative potentials increase in the region of the TiH_2 fragment. This implies that the body of the buckyball readily participates in nucleophilic processes, while the TiH_2 adsorbate is available for electrophilic processes. Meanwhile, the MEP distributions for the various $C_{59}TiH_2$ complexes are too similar

to permit discrimination among the given orientations of H_2 . In short, the MEP distributions indicate that the $C_{60}TiH_2$ complexes with H_2 oriented parallel to the x - and y -axes of fullerene are the most suitable configurations for hydrogen storage, based on the recommended adsorption energy range.

Polarizability and hyperpolarizability

The electronic dipole moments, molecular polarizabilities, anisotropies of polarizability, and first hyperpolarizabilities of the present complexes were investigated. The polarizability and hyperpolarizability characterize the response of a system in an applied electric field, and determine the strength of molecular interactions as well as the cross-sections of different scattering and collision processes. The electron in the p_z orbital of each sp^2 hybridized carbon atom in the fullerene will form π bonds with the neighboring p_z electrons. These π electrons are delocalized, resulting in high electronic polarizability. The significance of the hyperpolarizability and the first hyperpolarizability of a molecular system is dependent on the efficiency of electron transfer between the donor (Ti) and the acceptor (C_{60}), as this is key to intramolecular charge transfer [40–44].

The polarizability and hyperpolarizability tensors ($\alpha_{xx}, \alpha_{xy}, \alpha_{yy}, \alpha_{xz}, \alpha_{yz}, \alpha_{zz}$ and $\beta_{xxx}, \beta_{xxy}, \beta_{xyy}, \beta_{yyy}, \beta_{xxz}, \beta_{xyz}, \beta_{yyz}, \beta_{xzz}, \beta_{yzz}, \beta_{zzz}$) can be obtained by the finite-field, sum-over-states, and coupled perturbed Hartree–Fock methods. However, applying the previous methods with large basis sets to fullerenes such as C_{60} is too computationally expensive. Here, we compute the polarizability and hyperpolarizability tensors as

Fig. 6 Molecular electrostatic potential (MEP) surfaces of $C_{60}TiH_2$ and $C_{59}TiH_2$ complexes

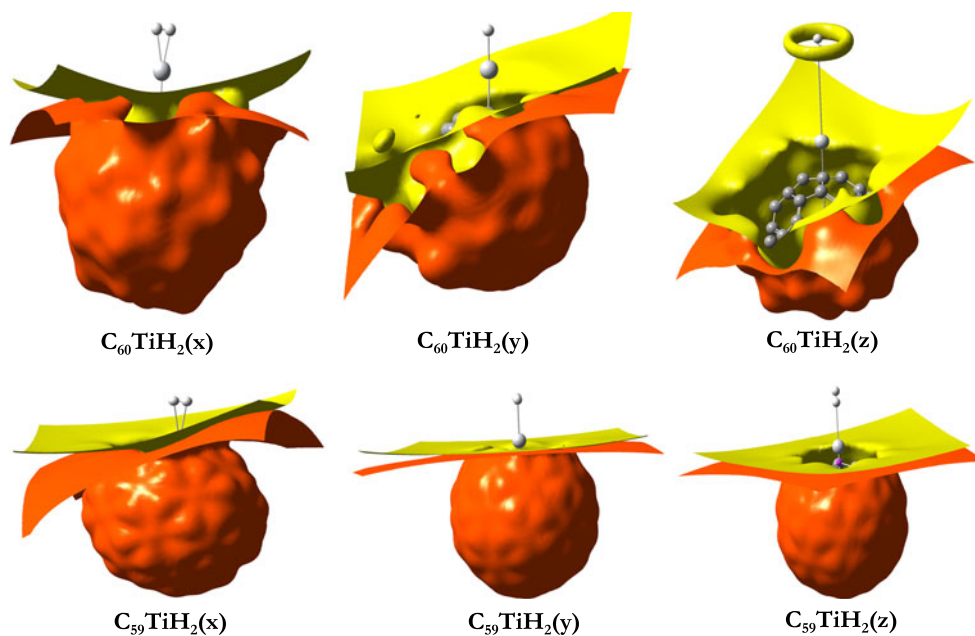


Table 5 The mean polarizability (α), anisotropy of polarizability ($\Delta\alpha$), dipole moment (μ), and the average value of the first hyperpolarizability (β) for $C_{60}TiH_2$ complexes

	α_{xx}	α_{xy}	α_{yy}	α_{xz}	α_{yz}	α_{zz}	α	$\Delta\alpha$	μ_x	μ_y	μ_z	μ
$C_{60}TiH_2(x)$	552.3	-74.3	678.2	-82.8	187.6	739.4	656.6	412.3	0.24	-0.57	-0.65	0.90
$C_{60}TiH_2(y)$	554.58	-77.06	684.9	-84.9	195.8	748.9	662.8	428.8	0.09	-0.94	-0.59	1.11
$C_{60}TiH_2(z)$	560.4	-85.5	699.1	-97.2	208.3	774.7	678.0	464.6	0.05	-0.48	-0.48	0.68
	β_{xxx}	β_{xxy}	β_{xyy}	β_{yyy}	β_{xzz}	β_{xyz}	β_{yzz}	β_{zzz}	β_{xzz}	β_{yzz}	β_{zzz}	$\beta_{ }$
$C_{60}TiH_2(x)$	409.4	-526.8	-414.81	-2727.1	-923.0	-647.4	-683.7	-376.2	-197.1	-1278.9	-1731.4	
$C_{60}TiH_2(y)$	385.6	-545.8	-429.1	-2815.6	-978.1	-775.5	-552.7	-351.1	132.4	-1390.8	-1753.0	
$C_{60}TiH_2(z)$	1182.1	-62.9	-1586.1	-155.4	-413.0	-2200.7	2420.1	-1948.6	3611.0	2552.0	2735.5	

Table 6 The mean polarizability (α), anisotropy of polarizability ($\Delta\alpha$), dipole moment (μ), and the average value of the first hyperpolarizability (β) for $C_{59}TiH_2$ complexes

	α_{xx}	α_{xy}	α_{yy}	α_{xz}	α_{yz}	α_{zz}	α	$\Delta\alpha$	μ_x	μ_y	μ_z	μ
$C_{59}TiH_2(x)$	488.5	-17.3	509.4	-19.5	38.6	524.7	507.5	86.6	0.72	-2.1	-2.5	3.34
$C_{59}TiH_2(y)$	488.2	-17.4	509.2	-19.1	38.4	524.6	507.4	86.2	0.70	-2.1	-2.5	3.34
$C_{59}TiH_2(z)$	486.2	-18.8	512.0	-21.8	42.3	530.0	509.4	96.5	0.80	-2.16	-2.43	3.35
	β_{xxx}	β_{xxy}	β_{xyy}	β_{yyy}	β_{xzz}	β_{xyz}	β_{yzz}	β_{zzz}	β_{xzz}	β_{yzz}	β_{zzz}	$\beta_{ }$
$C_{59}TiH_2(x)$	368.4	-466.6	435.8	-1053.6	-492.0	478.7	-914.6	677.2	-1016.0	-1615.0	-1813	
$C_{59}TiH_2(y)$	354.8	-449.4	417.2	-1029.6	-474.2	459.3	-898.8	656.2	-1003.6	-1620.0	-1795.8	
$C_{59}TiH_2(z)$	385.8	-470.8	452.9	-1174.7	-511.2	509.2	-1063.2	763.2	-1240.2	-2031.6	-2163.6	

Table 7 Infrared and Raman parameters, and the P and U depolarizations, of H₂ (H(62)–H(63)) in C₆₀TiH₂ complexes in the gas phase, as calculated at the B3LYP/6-31G(d) level of theory

	Infrared (IR)			Raman scattering activity (Å ⁴ /amu)	P depolarization	U depolarization
	Frequency (cm ⁻¹)	Force constant (m dyne/Å)	Dipole strength (10 ⁻⁴⁰ esu ² cm ²)			
C ₆₀ TiH ₂ (x)	3989	9.45	6500	1989	0.716	0.835
C ₆₀ TiH ₂ (y)	3813	8.64	7000	2154	0.705	0.827
C ₆₀ TiH ₂ (z)	5114	15.53	350	306	0.333	0.499

numerical derivatives of the dipole moment, obtained from a frequency job output file of the Gaussian software package.

The definition [45] of the mean polarizability is

$$\alpha = \frac{1}{3}(\alpha_{xx} + \alpha_{yy} + \alpha_{zz}), \quad (9)$$

while that for the anisotropy of polarizability is

$$\Delta\alpha = \frac{1}{\sqrt{2}} \left[(\alpha_{xx} - \alpha_{yy})^2 + (\alpha_{yy} - \alpha_{zz})^2 + (\alpha_{zz} - \alpha_{xx})^2 + 6\alpha_{xz}^2 + 6\alpha_{xy}^2 + 6\alpha_{yz}^2 \right]^{\frac{1}{2}} \quad (10)$$

and that for the average value of the first of the first hyperpolarizability is

$$\langle\beta\rangle = \left[(\beta_{xxx} + \beta_{xyy} + \beta_{xzz})^2 + (\beta_{yyy} + \beta_{yzz} + \beta_{yxx})^2 + (\beta_{zzz} + \beta_{zxx} + \beta_{zyy})^2 \right]^{\frac{1}{2}} \quad (11)$$

The total dipole moment can be calculated using the following equation:

$$\mu_{\text{tot}} = \left(\mu_x^2 + \mu_y^2 + \mu_z^2 \right)^{\frac{1}{2}}, \quad (12)$$

where μ_i ($i=x, y, z$) is the electronic dipole moment.

The calculated parameters described above for the C₆₀TiH₂ and C₅₉TiH₂ complexes are presented in Tables 5 and 6. For the C₆₀TiH₂ complexes (Table 5), several facts emerge:

- (i) The polarizability α is dominated by the term α_{zz} , and the polarizability terms α_{xy} and α_{xz} are not significantly affected by the orientation of H₂ with respect to the x -, y -, and z -axes of C₆₀. The smallest values of α and $\Delta\alpha$ are found for the x - and y -orientations.
- (ii) The average value of the hyperpolarizability $\langle\beta\rangle$ is dominated by the term β_{yyy} for the x - and y -orientations of H₂, and by the term β_{zzz} for the z -orientation. The term β_{yzz} of the x - and y -orientations and the term β_{yyy} for the z -orientation are not significantly affected. Except for β_{xxx} , β_{xyy} , and β_{xzz} , the smallest values of β are seen for the x - and y -orientations.
- (iii) The resultant dipole moment μ is dominated by the components μ_y and μ_z . The component μ_x is not significantly affected by the orientation of H₂. The largest values of μ are found for the x - and y -orientations of H₂.

For C₅₉TiH₂ complexes (Table 6), the following facts emerge:

- (i) The polarizability α is dominated by the term α_{zz} , and the polarizability terms α_{xy} and α_{xz} are not significantly affected by the orientation of H₂ with respect to the x -, y -, and z -axes of C₅₉. The smallest values of α and $\Delta\alpha$ are found for the x - and y -orientations.
- (ii) The average value of the hyperpolarizability $\langle\beta\rangle$ is dominated by the term β_{zzz} for all three orientations of H₂. The term β_{xxx} is not significantly affected by the orientation of H₂.
- (iii) The resultant dipole moments μ of the three considered orientations of H₂ are nearly identical. Further inspection of Tables 5 and 6 indicates that while the resultant

Table 8 Infrared and Raman parameters, and the P and U depolarizations, of H₂ (H(62)–H(63)) in C₅₉TiH₂ complexes in the gas phase, as calculated at the B3LYP/6-31G(d) level of theory

	Infrared (IR)			Raman scattering activity (Å ⁴ /amu)	P depolarization	U depolarization
	Frequency (cm ⁻¹)	Force constant (m dyne/Å)	Dipole strength (10 ⁻⁴⁰ esu ² cm ²)			
C ₅₉ TiH ₂ (x)	4617	12.66	100	925	0.254	0.405
C ₅₉ TiH ₂ (y)	4770	13.51	100	893	0.256	0.407
C ₅₉ TiH ₂ (z)	4782	13.58	400	1314	0.324	0.489

dipole moments μ of the $C_{59}TiH_2$ complexes are greater than those of the $C_{60}TiH_2$ complexes, the mean polarizability α and the anisotropy of polarizability $\Delta\alpha$ are significantly smaller.

The average value of the hyperpolarizability $\langle\beta\rangle$ and the values of its components are randomly distributed without clear trends. In short, the parameters α , $\Delta\alpha$, β , and μ depend on the orientation of H_2 , and orientations along the x - and y -axes of C_{60} are the most suitable for hydrogen storage, based on the recommended adsorption energy range.

Spectral characterization

A numerical harmonic vibrational analysis of the infrared spectrum of molecular hydrogen was carried out to find its strongest vibrational mode, and to characterize the H_2 orientation most suitable for hydrogen storage. Modes mixed with H_2 vibrations were not taken into account. The calculated infrared (IR) bands, force constants, dipole strengths, Raman (R) scattering activities, and the P and U depolarizations of H_2 in the $C_{60}TiH_2$ and $C_{59}TiH_2$ complexes are collected in Tables 7 and 8. For the $C_{60}TiH_2$ complexes (Table 7), inspection of the IR frequencies shows that all of the bands shift in position and intensity according to the orientation of H_2 . While a down shift of the band at frequency ($3,989\text{ cm}^{-1}$) assigned to (H_2 str. H(62)–H(63)) with force constant (9.45 m dyne/\AA) and dipole strength ($6,500 \times 10^{-40}\text{ esu}^2\text{ cm}^2$) is observed upon changing H_2 orientation from the x -direction to the y -direction, an up shift is observed upon changing H_2 orientation from the y -direction to the z -direction. An opposite behavior is observed for Raman (R) scattering activity ($1989\text{ A}^4/\text{amu}$), Pdepolarization (0.716), and U-depolarization (0.835) assigned to (H_2 str. H(62)–H(63)). These effects can be attributed to the interaction between H_2 and the Ti atom deposited on top of a C site in C_{60} . As shown, the highest values for the spectral parameters (except the force constants) occur for the x - and y -orientations of H_2 . Thus, the IR and R spectral parameters indicate that the complexes with H_2 oriented parallel to the x - and y -axes of C_{60} are the most suitable for hydrogen storage, based on the recommended adsorption energy range. For $C_{59}TiH_2$ complexes (Table 8), there are continuous increases in the IR frequency of the band at 4617 cm^{-1} for $C_{59}TiH_2(x)$ and the R band that has a scattering activity of $925\text{ \AA}^4/\text{AMU}$ for $C_{59}TiH_2(x)$, in contrast to what is seen for the $C_{60}TiH_2$ complexes. Apart from the IR dipole strength, there are parallel increases in the other spectral parameters too. Thus, the results indicate that the IR and R spectra depend on orientation of the interaction between H_2 and TiC_{59} . Comparison between the two types of complexes (with and without a C vacancy) indicates that only the IR frequencies and force constants of the defect-free $C_{60}TiH_2$

Table 9 Theoretical chemical shifts in ^1H NMR in (ppm) with reference shielding of 32.598 ppm, calculated at the HF/LANL2MB level of theory, for $C_{60}TiH_2$ complexes

	Atom	^1H NMR ^a	^1H NMR ^b	^1H NMR ^c
$C_{60}TiH_2(x)$	H(62)	−66.0	−66.5	98.2
	H(63)	−94.0	−95.0	126.5
$C_{60}TiH_2(y)$	H(62)	−57.5	−58.25	90.0
	H(63)	−79.0	−80.0	112.0
$C_{60}TiH_2(z)$	H(62)	5.22	4.70	27.19
	H(63)	5.10	4.45	27.43

^a With respect to TMS at HF/6-31G(d) GIAO

^b With respect to TMS at B3LYP/6-311+G(2d,p) GIAO

^c No reference

complexes are greater than those of the defect-containing $C_{59}TiH_2$ complexes.

It is known that accurate predictions of molecular geometries are needed to perform reliable calculations of magnetic properties. We therefore attempted to characterize the orientation of H_2 with respect to the Ti-functionalized fullerenes in terms of their ^1H NMR spectra. The calculated chemical shifts (ppm) of ^1H with respect to TMS at the HF/6-31G(d) GIAO, TMS at the B3LYP/6-311+G(2d,p) GIAO, and with no reference in for the $C_{60}TiH_2$ and $C_{59}TiH_2$ complexes in the gas phase, calculated at the HF/LANL2MB level of theory, are collected in Tables 9 and 10. Based on the data calculated for the complexes $C_{60}TiH_2$ (Table 9), the H(62) protons of the complexes $C_{60}TiH_2(x)$ and $C_{60}TiH_2(y)$ show much smaller chemical shifts than the H(63) protons with respect to TMS at HF/6-31G(d) GIAO, TMS at B3LYP/6-311G(2d,p), and with no reference, in contrast to what is seen for the complex $C_{60}TiH_2(z)$. Moreover, the largest chemical shifts are observed for the H_2 protons of the complexes $C_{60}TiH_2(x)$ and $C_{60}TiH_2(y)$. However, for the complex $C_{60}TiH_2(z)$ with no reference, the

Table 10 Theoretical chemical shifts in ^1H NMR in ppm with reference shielding of 32.598 ppm, calculated at the HF/LANL2MB level of theory, for $C_{59}TiH_2$ complexes

	Atom	^1H NMR ^a	^1H NMR ^b	^1H NMR ^c
$C_{59}TiH_2(x)$	H(61)	0.09	−0.625	32.51
	H(62)	−0.51	−1.225	33.11
$C_{59}TiH_2(y)$	H(61)	0.08	−0.64	32.52
	H(62)	−0.67	−1.39	33.27
$C_{59}TiH_2(z)$	H(61)	0.03	−0.70	32.60
	H(62)	2.96	2.25	29.65

^a With respect to TMS at HF/6-31G(d) GIAO

^b With respect to TMS at B3LYP/6-311+G(2d,p) GIAO

^c No reference

chemical shift of the H(62) proton is smaller than that of the H(63) proton. These results for the ^1H NMR spectra of the $\text{C}_{60}\text{TiH}_2$ complexes indicate that orientations of H_2 parallel to the x - and y -axes of C_{60} are the most suitable orientations for hydrogen storage, based on the recommended adsorption energy range. Comparison between the defect-free $\text{C}_{60}\text{TiH}_2$ complexes (Table 9) and the defect-containing $\text{C}_{59}\text{TiH}_2$ complexes (Table 10) shows that the trends for both sets of complexes are identical, differing only in the magnitudes of the chemical shifts observed.

Conclusions

We have performed ab initio molecular electronic structure calculations within the framework of density functional theory to investigate the effect of creating a C vacancy in Ti-functionalized C_{60} fullerene on its adsorption of molecular hydrogen and on the orientation dependence of this interaction with molecular hydrogen. We studied the effects of changing the H_2 orientation on various physicochemical properties, including the adsorption energy, charge transfer, pairwise and non-pairwise additivity, frontier orbital band gaps and isosurface plots, density of states, as well as molecular electrostatic potential surfaces, dipole moments, polarizabilities and hyperpolarizabilities, and simulated IR, R, and ^1H NMR spectra. The preferential orientations of H_2 in the defect-free complexes were along the x - and y -axes of the fullerene, with adsorption energies of -0.23 and -0.21 eV, respectively. The defect-containing complexes do not reproduce adsorption energies within the energy range targeted by the DOE. While creating a C vacancy in the fullerene improves the adsorption energy of Ti, it reduces the adsorption energy of H_2 . Charge transfer occurs from Ti to the fullerene (from Ti $3d$ to C $2p$). The binding of H_2 is dominated by the support–metal interaction energy term $E(i)^{\text{C}_n\cdots\text{Ti}}$ and the role of fullerene is not restricted to supporting the metal. A significant reduction in the energy gap is observed when TiH_2 is adsorbed onto the pristine fullerene. The C_n fullerene readily participates in nucleophilic processes, while the adjacent TiH_2 fragment is available for electrophilic processes. The average value of the hyperpolarizability is dominated by β_{yyy} and the largest μ value. The physicochemical parameters can be used to distinguish between the H_2 -adsorption modes of the defect-free complex, whereas they cannot be used in this way for the defect-containing complex. The highest values of the infrared and Raman spectral parameters (except for the force constants) were found for the x - and y -orientations of H_2 . If fullerenes are to become the base materials of a hydrogen fuel cell technology, many improvements remain to be achieved either to the base materials such as fullerenes and carbon nanotubes, or to the hydrogen

storage technology. This goal can be achieved by identifying and characterizing all physicochemical contributions to the overall problem of hydrogen storage and systematically optimizing each one. Functionalization of fullerenes or carbon nanotubes, and developing new efficient methods for hydrogen storage at ambient temperature are just two kinds of improvements that can be achieved.

As hydrogen storage is one of the key challenges in the development of clean hydrogen energy, it is not surprising that considerable research efforts have focused on optimizing current hydrogen storage technologies. If fullerenes are to become the base materials used in hydrogen fuel cell technology, many improvements must be made. This goal can be achieved by identifying and characterizing all of the physicochemical contributions to the overall problem and systematically optimizing each one. The synergy between theory and experiment is making it easier to search for new hydrogen storage materials with particular properties.

References

- Li J, Furuta T, Goto H, Ohasi T, Fujiwara Y, Yip S (2003) *J Chem Phys* 119:2376
- Venkataraman NS, Sahara R, Mizuseki H, Kawazoe Y (2008) *J Phys Chem C* 112:19676–19679
- Khazaei M, Bahramy MS, Venkataraman NS, Mizuseki H, Kawazoe Y (2009) *J Appl Phys* 106:094303
- Jorio A, Dresselhaus G (2004) *Encyclopedia of physical science and technology*. Elsevier, Amsterdam, p. 315
- Subramoney S (2001) *Encyclopedia of physical science and technology*. Elsevier, Amsterdam, p. 941
- Venkataraman NS, Mizuseki H, Kawazoe Y (2009) *Nano* 4:253
- Chatt J, Duncanson L (1953) *J Chem Soc* 2939
- Zhao Y, Kim Y-H, Dilton AC, Heben MJ, Zhang SB (2005) *Phys Rev Lett* 94:155504
- Yildirim T, Iniguez J, Ciraci S (2005) *Phys Rev B* 72:153403
- Sun G, Wang Q, Jena P, Kawazoe Y (2005) *J Am Chem Soc* 127:14582
- Hay PJ, Wadt WR (1985) *J Chem Phys* 82:299
- Petersson GA, Al-Laham MA (1991) *J Chem Phys* 94:6081
- Martyin RL, Illas F (1997) *Phys Rev Lett* 79:1539
- Moreira IPR, Illas F, Martin RL (2002) *Phys Rev B* 65:155102
- Caballol R, Castell O, Illas F, Malrieu JP, Moreira IPR (1997) *J Phys Chem A* 101:7860
- Ricca A, Bauschlicher CW (1994) *J Phys Chem* 98:12899
- Russo TV, Martin RI, Hay PJ (1995) *J Chem Phys* 102:8023
- Siegbahn PE, Crabtree RH (1997) *J Am Chem Soc* 119:3103
- Pacchioni G (2001) In: Woodruff DP (ed) *The chemical physics of solid surfaces, vol 9: oxide surfaces*. Elsevier, Amsterdam
- Pacchioni G (2000) *Surf Rev Lett* 7:277
- Frisch MJ, et al. (2009) *Gaussian 09*. Gaussian, Inc., Pittsburgh
- Strobel R, Garche J, Moseley PT, Jorissen L, Wolf G (2006) *J Power Sources* 159:781
- Yildirim T, Ciraci S (2005) *Phys Rev Lett* 94:175501
- Shalabi AS, Kamel KA, Assem MM (1995) *Theor Chem Acta* 91:73
- Shalabi AS, Nour EM, Abdel Halim WS (2000) *Int J Quant Chem* 76:10

26. Abdel Halim WS, Assem MM, Shalabi AS, Soliman KA (2009) *Appl Surf Sci* 255:7547
27. Shalabi AS, Assem MM, Abdel Aal S, Soliman KA (2012) *J Nanopart Res* 14:892
28. Lopez N, Illas F, Rösch N, Pacchioni G (1999) *J Chem Phys* 110:48739
29. Fukui K (1982) *Science* 218:747
30. Ashra RS, Klemm E (2005) *J Polym Sci A43*:6445
31. Tarakeshwar P, Kim DM (2005) *J Phys Chem B* 109:7601
32. Wang DL, Shen HT, Gu HM, Zhai YC (2006) *J Mol Struct Theochem* 776:47
33. Naray-Szabo G, Ferenczy GG (1995) *Chem Rev* 95:829
34. Murray JS, Politzer P (1998) Chapter 3. In: Spase AM (ed) *Molecular orbital calculations for biological systems*. Oxford University Press, New York
35. Wang X, Li X, Li H (2008) *Phys Lett A* 372:6677
36. Parikth K, Cattanatch K, Rao R, Suh DS, Wu A, Manohar SK (2006) *Sens Actuators B* 113:55
37. Wang D, Sun X, Xin G, Hou D (2010) *Physica B* 405:2745
38. Ragavachari K, Zhang B, Pople JA, Johnson BG, Gill PMW (1994) *Chem Phys Lett* 220:385
39. Politzer P, Truhlar DG (eds) (1981) *Chemical applications of atomic and molecular electrostatic potentials*. Plenum, New York
40. Ditchfield R (1972) *J Chem Phys* 56:5688
41. Wolinski K, Hinton JF, Pulay P (1990) *J Am Chem Soc* 112:8251
42. Prasad O, Sinha L, Misra N, Narayan V, Kumar N, Pathak J (2010) *J Mol Struct* 940:82
43. Zhang R, Du B, Sun G, Sun Y (2010) *Spectrochim Acta A* 75:1115
44. Pihlaja K, Kleinpeter E (eds) (1994) *Carbon 13 chemical shifts in structure and spectrochemical analysis*. VCH, Deerfield Beach
45. Cinar M, Coruh A, Karabacak M (2011) *Spectrochim Acta A* 83:561